Journal of Power Sources 196 (2011) 8463–8471

Contents lists available at ScienceDirect

Journal of Power Sources

journal homepage: www.elsevier.com/locate/jpowsour

Thermodynamic analysis of a new combined cooling, heat and power system driven by solid oxide fuel cell based on ammonia–water mixture

Shaolin Ma[a,b], Jiangfeng Wang[a,*], Zhequan Yan[a], Yiping Dai[a], Bingheng Lu[a]

[a] Xi'an Jiaotong University, Xi'an 710049, China
[b] Dongfang Steam Turbine Works, Deyang 618201, China

ARTICLE INFO

Article history:
Received 9 March 2011
Received in revised form 2 June 2011
Accepted 2 June 2011
Available online 13 June 2011

Keywords:
Absorption
Ammonia–water mixture
Combined cooling
Heat and power
Kalina cycle
Parametric analysis
Solid oxide fuel cell

ABSTRACT

Although a solid oxide fuel cell combined with a gas turbine (SOFC-GT) has good performance, the temperature of exhaust from gas turbine is still relatively high. In order to recover the waste heat of exhaust from the SOFC-GT to enhance energy conversion efficiency as well as to reduce the emissions of greenhouse gases and pollutants, in this study a new combined cooling, heat and power (CCHP) system driven by the SOFC is proposed to perform the trigeneration by using ammonia–water mixture to recover the waste heat of exhaust from the SOFC-GT. The CCHP system, whose main fuel is methane, can generate electricity, cooling effect and heat effect simultaneously. The overall system performance has been evaluated by mathematical models and thermodynamic laws. A parametric analysis is also conducted to examine the effects of some key thermodynamic parameters on the system performance. Results indicate that the overall energy conversion efficiency exceeds 80% under the given conditions, and it is also found that the increasing the fuel flow rate can improve overall energy conversion efficiency, even though both the SOFC efficiency and electricity efficiency decrease. Moreover, with an increased compressor pressure ratio, the SOFC efficiency, electricity efficiency and overall energy conversion efficiency all increase. Ammonia concentration and pressure entering ammonia–water turbine can also affect the CCHP system performance.

1. Introduction

Great consumption of fossil fuels, global warming and environment deterioration has attracted many researchers to find more efficient methods of energy conservation, and reducing greenhouse gas emissions as well as pollutants. Combined cooling, heating, and power (CCHP), which is also known as trigeneration, is a booming new technology for efficient and clean production of energy. It can generate simultaneously the mechanical power (often converted to electricity), heating and cooling from one primary fuel. Wu and Wang [1] performed an extensive and intensive review of CCHP systems. This literature survey shows that most CCHP systems use fossil fuel as primary heat source. Currently, CCHP technologies usually use steam turbines, internal combustion engines, gas turbines, micro gas turbines, Stirling engines or fuel cells as a primary driver to perform the trigeneration. Among them, the CCHP system driven by fuel cells has achieved higher energy conversion efficiency because the efficiency of fuel cell is not subject to the limitation of Carnot efficiency.

Solid oxide fuel cell (SOFC) is considered as one of the most promising technologies to directly convert fuel chemical energy into electricity. It operates at high temperature and produces great waste heat, therefore it is generally coupled with a gas turbine (GT) or an organic Rankine cycle (ORC) as the bottom cycle to increase the overall efficiency by recovering waste heat from SOFC. Many researchers have studied the performance of the hybrid SOFC-GT power system [2–16] or combined SOFC-ORC power system [17,18]. However, only a few of them concentrate on the performance analysis of CCHP systems driven by SOFC.

Burer et al. [19] conducted a thermo-economical optimization of a CCHP system comprising an SOFC-GT combined cycle, a heat pump, an additional gas boiler, a compression chiller and/or an absorption chiller. Their study mainly focused on the cost and CO_2 emission analysis by using multi-criteria optimization with an annual total cost of CCHP and annual CO_2 emission rate as the optimization objectives. Burer's study shows that the SOFC-GT system is an attractive economical and environmental solution. Liu et al. [20] proposed a CCHP system by integrating internal-reforming solid oxide fuel cell (IRSOC) with a zeolite/water adsorption chiller. They also investigated the performance of the system under different operating conditions and parameters. Yu et al. [21] analyzed

* Corresponding author at: Xi'an Jiaotong University, Institute of Turbomachinery, No. 28, Xianning West Road, Xi'an 710049, China. Tel.: +86 029 82668704; fax: +86 029 82668704.
E-mail address: jfwang@mail.xjtu.edu.cn (J. Wang).

0378-7753/$ – see front matter © 2011 Elsevier B.V. All rights reserved.
doi:10.1016/j.jpowsour.2011.06.008

Nomenclature

A_a	active surface area, m^2
E_r	reversible cell voltage, V
F	Faraday constant, C mol^{-1}
ΔG^0	Gibbs free energy at standard pressure (1 atm) and temperature, J mol^{-1}
h	enthalpy, kJ kg^{-1}
i	current density, A m^{-2}
i_0	exchange current, A m^{-2}
K_p	equilibrium constant of the shifting reaction
LHV	lower heating value of the fuel, kJ kg^{-1}
$\dot{m}$	mass flow rate, kg s^{-1}
$\dot{n}$	molar flow rate, mol s^{-1}
n_e	number of electrons participating in the electrochemical reaction
p	partial pressure for different species, bar
P_0	ambient pressure, bar
Q	heat rate, kW
R	universal gas constant, J mol^{-1} K^{-1}
R_i	resistivity, Ω
T	temperature, K
V_{loss}	voltage loss, V
V	cell voltage, V
W	power, kW
x	extent of the reforming reaction for methane, mol s^{-1}
X	ammonia concentration
y	extent of the shifting reaction, mol s^{-1}
z	extent of electrochemical reaction, mol s^{-1}

Greek letters

α	charge transfer coefficient
β	fuel utilization factor
δ_i	thickness, cm
η	efficiency
κ	isentropic exponent
π	pressure ratio
ρ_i	material resistivity, Ω cm^{-1}

Subscripts

ABS1	absorber 1
ABS2	absorber 2
act	activation
C	condenser
comp	compressor
cont	concentration
E	evaporator
T	extraction ammonia–water turbine
gas	flue gas produced after combustion
GT	gas turbine
H	heater
in	inlet
LHV	as-received basis low heat value
ohm	Ohmic
out	outlet
s	isentropic process
sh	sensible heat
tri	trigeneration

a total energy system incorporating a solid oxide fuel cell and an absorption chiller driven by exhaust gas to provide power, cooling and/or heating simultaneously. Their parametric analysis shows that both electrical efficiency and total efficiency of the TES have maximum values with variation of the fuel utilization factor.

Al-Sulaiman et al. [22] analyzed a CCHP system based on a SOFC and ORC. In this CCHP system, ORC as a bottoming cycle was used to recover the waste heat from the SOFC to generate power; the exhaust gas of organic turbine was applied to provide heat, and a single-effect absorption chiller was employed to provide cooling capacity. The study reveals that, compared with only power system, efficiency increases by at least 22% when a trigeneration system is used. They [23] also conducted an exergy analysis of the trigeneration plant. A 3–25% increase in exergy efficiency can be observed if trigeneration is applied instead of only a power system.

It is known that the waste heat from SOFC or SOFC-GT is a sensible heat source, whose temperature decreases during the heat ejection process. In order to obtain a small temperature difference for a good thermal match between the variable temperature heat source and the working fluid which reduces irreversible loss in the heat transfer process consequently, binary component mixtures are often used, taking account of their characteristic of variable boiling temperature during the boiling process. The ammonia–water mixture is a typical binary mixture which has been successfully used in Kalina cycle [24] to improve evidently the performance of power system. It not only has excellent thermo-physical properties, but also has an environmentally friendly substance.

In this study, a new combined cooling, heat and power system driven by the solid oxide fuel cell is proposed to perform the trigeneration by using the ammonia–water mixture to recover the waste heat of exhaust from SOFC-GT. A mathematical model has been developed to simulate the new CCHP system under steady-state conditions, and a parametric analysis is conducted to examine the effects of some key thermodynamic parameters on the combined system performance.

2. System description

Fig. 1 illustrates a schematic diagram of the new CCHP system driven by a solid oxide fuel cell based on the ammonia–water mixture, which can produce power, heating and refrigeration simultaneously from one fuel source, such as natural gas. The proposed system consists of an SOFC, an after-burner, a gas turbine, a waste heat boiler, an ammonia–water turbine, some heat exchangers, a rectifier, and other related components.

It can been seen from Fig. 1, the fuel and the air are compressed up to a SOFC stack operating pressure by the fuel and air compressors, and preheated in corresponding preheaters by exhaust of a gas turbine. In addition, after being pressurized by the pump, the water is preheated to generate the superheated steam in the corresponding preheater by exhaust of a gas turbine then it is mixed with the fuel to produce the mixture that will drive the internal reforming reaction.

The preheated air is fed to the cathode of the SOFC as well as the mixture of steam, while fuel is fed to the SOFC anode. The electrochemical reaction occurs to produce DC current which is converted into the AC current by an inverter.

After the electrochemical reaction in the SOFC stack has finished, the excess air out of the cathode and the unreacted fuel out of the anode combust completely in an after-burner to generate the combustion gas under high temperature and pressure, which is expanded through a gas turbine to produce power. The exhaust gas from gas turbine is sequentially used to preheat the air, fuel and water respectively.

The ammonia–water mixture is applied as working fluid to absorb the heat from exhaust gas in a waste heat boiler to produce superheated ammonia–water vapor, which can reduce the heat transfer irreversibility due to mixture's variable temperature vaporized characteristic.

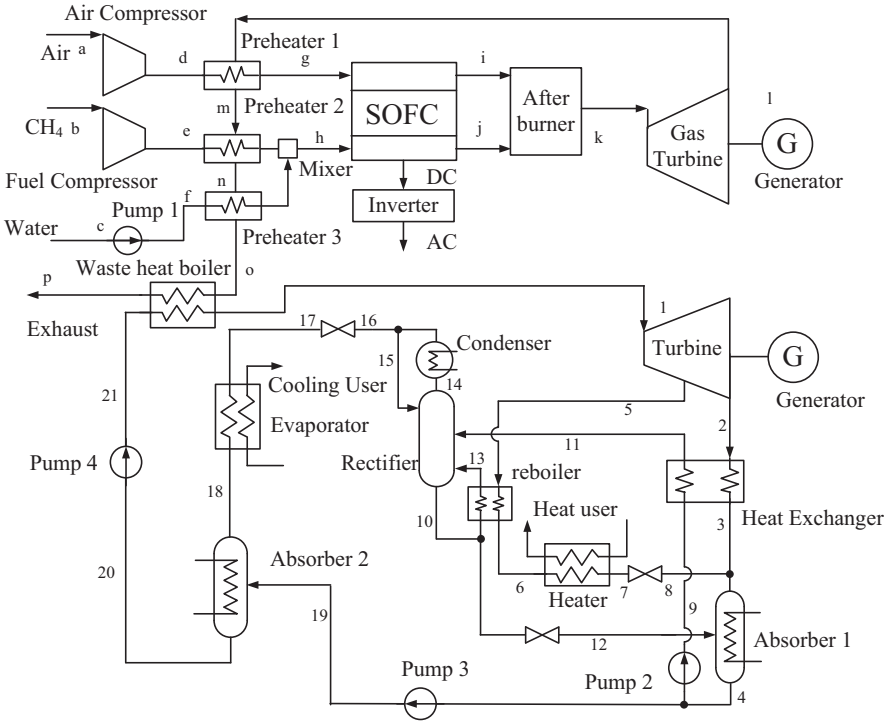

Fig. 1. Schematic diagram of the new CCHP system driven by SOFC.

In the next phase, the superheated ammonia–water is expanded through the extraction turbine to generate electricity. An extraction ammonia–water vapor coming from extraction turbine is used to heat a rectifier, and then enters a heater to provide heat for heat users. Then, the extraction stream is throttled to a low pressure across a throttling valve and is mixed with the turbine exhaust coming from a heat exchanger where one stream of ammonia–water basic solution is heated before it is fed to the rectifier. The mixture of two streams is sent to absorber 1, which is diluted with a weak solution coming from the rectifier. It is condensed in the absorber 1 by cooling water to form the ammonia–water basic solution.

One stream of the ammonia–water basic solution is pumped into the rectifier after being heated by the turbine exhaust gas. In the rectifier, the ammonia–water basic solution is separated into a weak solution and ammonia-rich vapor. The weak solution is throttled by a throttling valve and sent to absorber 1, and the ammonia-rich vapor is condensed to liquid in a condenser. Some ammonia-rich liquid returns to the rectifier, and the rest is then throttled by a throttling valve to a low-pressure state and enters an evaporator. This stream, which is almost pure ammonia, evaporates completely in the evaporator for cooling.

The other stream of ammonia–water basic solution is pumped into absorber 2 where it is used to absorb the saturated vapor from the evaporator using cooling water. The condensed ammonia–water liquid is then pumped to waste heat boiler to complete the cycle.

3. Mathematical model

3.1. SOFC model

In present study, some assumptions are employed to simplify the analysis of SOFC:

(1) The system reaches steady state.
(2) Air in the SOFC consists of 79% N_2 and 21% O_2.
(3) Chemical reaction reaches equilibrium state.
(4) Pressure at the anode and the cathode of the SOFC is constant and equal.
(5) Flow temperature at the inlet of the air and fuel channels in SOFC stack is constant and equal.
(6) Flow temperature at the exit of the air and fuel channels in SOFC stack is constant and equal to operation temperature of the SOFC.
(7) The unreacted gases are assumed to be fully oxidized in the after-burner.
(8) Radiation heat transfer between gas channels and solid structure is neglected.
(9) Contact resistances are negligible.
(10) Pressure change at SOFC is negligible.

For a SOFC system with natural gas fueled, either internal reforming or external reforming is needed. The use of an internal reformer can be a better choice due to its relatively low cost. The reaction mechanisms that occur within the anode and cathode of the solid oxide fuel cell can be written as follows.

Reforming:

$$CH_4 + H_2O = 3H_2 + CO \quad (1)$$

Shifting:

$$CO + H_2O = H_2 + CO_2 \quad (2)$$

Electrochemical:

$$\frac{1}{2}O_2 + H_2 = H_2O \quad (3)$$

Assuming that the methane is fully converted and the reforming reaction is completely developed due to the very high temperature condition and the catalytic effect of the anode materials. The shifting reaction is considered to reach thermodynamic equilibrium, with an equilibrium constant being given by:

$$K_p = \frac{p_{CO_2} \cdot p_{H_2}}{p_{CO} \cdot p_{H_2O}} \quad (4)$$

$$\log\ K_p = AT_{\text{sofc}}^4 + BT_{\text{sofc}}^3 + CT_{\text{sofc}}^2 + DT_{\text{sofc}} + E \tag{5}$$

where A, B, C, D and E are the constant values, given in [4].

The molar flow rates of the reaction in Eqs. (1)–(3), are x, y, z, respectively. The mass balance between inlet and exit of SOFC is given as follows:

$$\dot{n}_{\text{CH}_4,\text{in}} = x \tag{6}$$

$$\dot{n}_{\text{H}_2\text{O},\text{in}} = 2.5x \tag{7}$$

$$\dot{n}_{\text{H}_2,\text{out}} = 3x + y - z \tag{8}$$

$$\dot{n}_{\text{CO},\text{out}} = x - y \tag{9}$$

$$\dot{n}_{\text{CO}_2,\text{out}} = y \tag{10}$$

$$\dot{n}_{\text{H}_2\text{O},\text{out}} = 2.5x - x - y + z \tag{11}$$

$$z = \beta(3x + y) \tag{12}$$

where the variable $\dot{n}$ is the molar flow rate at the inlet or outlet of the SOFC, β is fuel utilization factor.

The cell voltage produced by the SOFC is defined as:

$$V_{\text{sofc}} = E_{\text{r}} - V_{\text{loss}} \tag{13}$$

The reversible cell voltage can be obtained from the Nernst equation as:

$$E_{\text{r}} = -\frac{\Delta G^0}{n_{\text{e}}F} + \frac{RT_{\text{sofc}}}{n_{\text{e}}F}\ln\left(\frac{p_{\text{H}_2}\sqrt{p_{\text{O}_2}}}{p_{\text{H}_2\text{O}}}\right) \tag{14}$$

where ΔG^0 is the Gibbs free energy at the standard pressure and temperature, n_{e} is the number of electrons participating in the electrochemical reaction, T_{sofc} is the fuel cell temperature at the exit of the fuel cell, p is the partial pressure of different reactants.

The voltage loss is expressed as:

$$V_{\text{loss}} = V_{\text{act}} + V_{\text{ohm}} + V_{\text{cont}} \tag{15}$$

The anodic and cathodic activation overvoltages can be calculated from the well-known Butler–Volmer equation [25]:

$$i = i_0\left\{\exp\left(\alpha\frac{n_{\text{e}}FV_{\text{act}}}{RT_{\text{sofc}}}\right) - \exp\left[-(1-\alpha)\frac{n_{\text{e}}FV_{\text{act}}}{RT_{\text{sofc}}}\right]\right\} \tag{16}$$

where i is the current density, i_0 known as the exchange current is the forward and reverse electrode reaction rate at the equilibrium potential, α is the charge transfer coefficient and its value is usually 0.5 for a great variety of electrode materials. Hence,

$$V_{\text{act}} = \frac{2RT_{\text{sofc}}}{n_{\text{e}}F}\sinh^{-1}\left(\frac{i}{2i_0}\right) \tag{17}$$

The exchange current density for anode and cathode can be determined by semi-empirical equations [25]. If the SOFC operates in low activation polarization conditions, Eq. (16) can be approximated in a linear form [26]:

$$V_{\text{act}} = \frac{RT_{\text{sofc}}}{n_{\text{e}}F}\cdot\frac{i}{i_0} \tag{18}$$

If the SOFC operates in high activation polarization conditions, it is possible to neglect the second term in Eq. (16) and write the relation known as Tafel's law:

$$V_{\text{act}} = \frac{RT_{\text{sofc}}}{n_{\text{e}}F\alpha}\cdot\ln\left(\frac{i}{i_0}\right) \tag{19}$$

Assuming a series arrangement, the ohmic overvoltage can be calculated by summing over all of the components of the cell (anode, cathode, electrolyte, interconnects). The ohmic loss is determined by:

$$V_{\text{ohm}} = i\sum R_i = i\sum \delta_i\rho_i = i\sum \delta_i\cdot A_i\exp\left(\frac{B_i}{T_{\text{sofc}}}\right) \tag{20}$$

where the values of A_i, B_i, and δ_i are given in [7].

It is assumed that the effect of the concentration polarization is negligibly small against the effects of the other polarization. This assumption is considered to be reasonable, because diffusion of reactants through the electrodes is sufficiently fast under high temperature operations [3]. At a high operating temperature of the SOFC, the concentration loss can be neglected because diffusion is a very efficient process.

The current density and current are defined respectively as:

$$i = \frac{zn_{\text{e}}F}{A_{\text{a}}} \tag{21}$$

$$I_{\text{sofc}} = i\cdot A_{\text{a}} = zn_{\text{e}}F \tag{22}$$

where I_{sofc} is the current density, A_{a} is the active surface area.

The power output of the SOFC is given by:

$$W_{\text{sofc}} = V_{\text{sofc}}\cdot I_{\text{sofc}} \tag{23}$$

3.2. Brayton cycle

It is assumed that the cycle reaches a steady state; the pressure drops in the after-burner, preheaters and connection tubes are neglected; there is no heat transfer with the environment; and the gas turbine and compressors have a given isentropic efficiency, respectively.

The heat entrained with the fuel and air entering the afterburner for combustion is composed of two parts; one is the sensible heat of fuel and air, and the other is the chemical heat. Assuming that the combustion process is performed adiabatically and completely [27], the heat balance before and after combustion is given as:

$$Q_{\text{CO,LHV}} + Q_{\text{H}_2,\text{LHV}} + Q_{\text{CO,sh}} + Q_{\text{H}_2,\text{sh}} + Q_{\text{O}_2,\text{sh}} + Q_{\text{N}_2,\text{sh}} = h_{\text{gas}} \tag{24}$$

where $Q_{\text{CO,LHV}}$ and $Q_{\text{H}_2,\text{LHV}}$ are the as-received basis low heat values of CO and H_2, respectively, $Q_{\text{CO,sh}}$, $Q_{\text{CO,sh}}$, $Q_{\text{O}_2,\text{sh}}$ and $Q_{\text{N}_2,\text{sh}}$ are the sensible heats of CO, H_2, O_2 and N_2, respectively, h_{gas} is the enthalpy of the flue gas produced after combustion.

The enthalpy of the flue gas produced after combustion can also be determined by:

$$h_{\text{gas}} = (\dot{n}_{\text{CO}_2}C_{\text{CO}_2} + \dot{n}_{\text{N}_2}C_{\text{N}_2} + \dot{n}_{\text{H}_2\text{O}}C_{\text{H}_2\text{O}})\cdot T_{\text{gas}} \tag{25}$$

where T_{gas} is the temperature of the flue gas after combustion, C_{CO_2}, C_{N_2} and $C_{\text{H}_2\text{O}}$ are the average constant pressure specific heats of CO_2, N_2 and H_2O at T_{gas}, respectively, $\dot{n}_{\text{CO}_2}$, $\dot{n}_{\text{N}_2}$ and $\dot{n}_{\text{H}_2\text{O}}$ are the mole flow rates of CO_2, N_2 and H_2O at T_{gas}, respectively.

The isentropic efficiency of the turbine is

$$\eta_{\text{GT}} = \frac{h_{\text{in}} - h_{\text{out}}}{h_{\text{in}} - h_{\text{out,s}}} \tag{26}$$

The generating power can be given as:

$$W_{\text{GT}} = \dot{m}_{\text{gas}}(h_k - h_l) \tag{27}$$

Assuming that CH_4 and air are ideal gases, isentropic compression in the compressors can be given as:

$$\frac{T_{\text{out,s}}}{T_{\text{in}}} = \pi^{((\kappa-1)/\kappa)} \tag{28}$$

The isentropic efficiencies are

$$\eta_{\text{comp}} = \frac{T_{\text{out,s}} - T_{\text{in}}}{T_{\text{out}} - T_{\text{in}}} \tag{29}$$

The actual compression powers are

$$W_{\text{comp}} = \frac{\dot{m}_{\text{in}}(\kappa/(\kappa-1))RT_0(\pi^{((\kappa-1/\kappa))} - 1)}{\eta_{\text{comp}}} \tag{30}$$

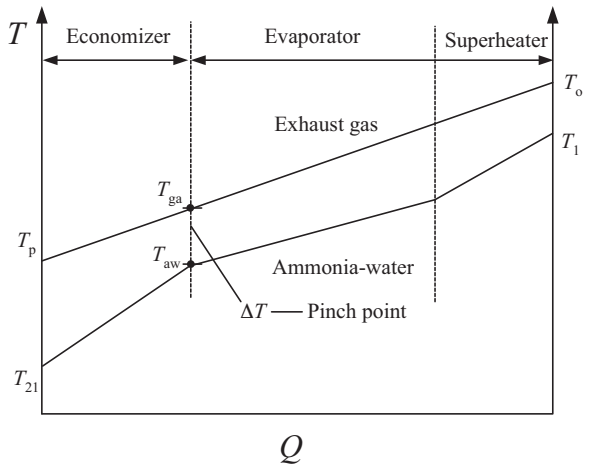

Fig. 2. Typical exhaust gas/ammonia–water temperature profile.

In the preheaters, the energy balance equations are

$$\dot{m}_{air}(h_{in,air} - h_{out,air}) = \dot{m}_{gas}(h_l - h_m) \quad (31)$$

$$\dot{m}_{fuel}(h_{in,fuel} - h_{out,fuel}) = \dot{m}_{gas}(h_m - h_n) \quad (32)$$

$$\dot{m}_{water}(h_{in,water} - h_{out,water}) = \dot{m}_{gas}(h_n - h_o) \quad (33)$$

3.3. Bottoming cycle using ammonia–water

To simplify the theoretical simulation, some assumptions are made as follows:

(1) The system reaches a steady state.
(2) The pressure drops through the waste heat boiler, absorbers, heater, heat exchanger, condenser, reboiler, rectifier, evaporator, and connection tubes are negligible.
(3) There is no heat transfer with the environment.
(4) The vapor stream from the rectifier is saturated vapor and the liquid stream from the rectifier is saturated liquid.
(5) The streams at the condenser outlet and absorber outlet are the saturated liquids, and the stream at the evaporator outlet is saturated vapor.
(6) The flows across the valves are isenthalpic.
(7) The pumps and ammonia–water turbine have a given isentropic efficiency, respectively.

The waste heat boiler consists of an economizer, an evaporator, and a superheater. Due to using ammonia–water mixture, in the vaporizing process, the more volatile ammonia tends to vaporize first at a lower temperature than the pure water. The temperature of the remaining saturated liquid rises as the ammonia concentration decreases. Thus, a better match between the heat rejection of exhaust gas and heat absorption of ammonia–water is performed using ammonia–water's characteristic of variable vaporizing temperature during the vaporizing process, as shown in Fig. 2.

Energy balance for superheater and evaporator is

$$\dot{m}_{gas}(h_o - h_{ga}) = \dot{m}_1(h_1 - h_{aw}) \quad (34)$$

Energy balance for the economizer is

$$\dot{m}_{gas}(h_{ga} - h_p) = \dot{m}_1(h_{aw} - h_{21}) \quad (35)$$

In the rectifier, the mass balance equation is

$$\dot{m}_{11} + \dot{m}_{13} + \dot{m}_{15} = \dot{m}_{14} + \dot{m}_{10} \quad (36)$$

and the ammonia mass balance equation is

$$\dot{m}_{11}X_{11} + \dot{m}_{13}X_{13} + \dot{m}_{15}X_{15} = \dot{m}_{14}X_{14} + \dot{m}_{10}X_{10} \quad (37)$$

In the condenser, the heat ejection is given by:

$$Q_C = \dot{m}_{14}(h_{14} - h_{16}) \quad (38)$$

In the reboiler, the energy balance equation is

$$\dot{m}_5(h_5 - h_6) = \dot{m}_{13}(h_{13} - h_{10}) \quad (39)$$

In the evaporator, the refrigeration output for user is given by:

$$Q_E = \dot{m}_{17}(h_{18} - h_{17}) \quad (40)$$

In the heater, the heat output for users is given by:

$$Q_H = \dot{m}_6(h_6 - h_7) \quad (41)$$

In absorber 1, the mass balance equation is

$$\dot{m}_3 + \dot{m}_8 + \dot{m}_9 = \dot{m}_4 \quad (42)$$

and the ammonia mass balance equation is

$$\dot{m}_3X_3 + \dot{m}_8X_8 + \dot{m}_9X_9 = \dot{m}_4X_4 \quad (43)$$

The energy balance equation is

$$Q_{ABS1} = \dot{m}_3h_3 + \dot{m}_8h_8 + \dot{m}_9h_9 - \dot{m}_4h_4 \quad (44)$$

In absorber 2, the mass balance equation is

$$\dot{m}_{18} + \dot{m}_{19} = \dot{m}_{20} \quad (45)$$

and the ammonia mass balance equation is

$$\dot{m}_{18}X_{18} + \dot{m}_{19}X_{19} = \dot{m}_{20}X_{20} \quad (46)$$

The energy balance equation is

$$Q_{ABS2} = \dot{m}_{18}h_{18} + \dot{m}_{19}h_{19} - \dot{m}_{20}h_{20} \quad (47)$$

The power output of extraction ammonia–water turbine is given by:

$$W_T = \dot{m}_1(h_1 - h_5) + \dot{m}_2(h_5 - h_2) \quad (48)$$

In the pumps, the isentropic efficiencies are

$$\eta_{PUMP} = \frac{h_{out,s} - h_{in}}{h_{out} - h_{in}} \quad (49)$$

The works input by the pumps are

$$W_{PUMP2} = \dot{m}_9(h_9 - h_4) \quad (50)$$

$$W_{PUMP3} = \dot{m}_{19}(h_{19} - h_4) \quad (51)$$

$$W_{PUMP4} = \dot{m}_{20}(h_{21} - h_{20}) \quad (52)$$

4. Performance criteria

The performance of the CCHP system can be evaluated by the SOFC electricity efficiency, electricity efficiency and overall energy conversion efficiency.

The SOFC electricity efficiency is calculated as follows:

$$\eta_{SOFC} = \frac{W_{sofc}}{\dot{m}_{fuel} \cdot LHV} \quad (53)$$

where LHV is the lower heating value of the fuel.

Electricity efficiency is calculated as follows:

$$\eta_{electricity} = \frac{W_{sofc} + W_{GT} + W_T - W_{comp} - W_{pump}}{\dot{m}_{fuel} \cdot LHV} \quad (54)$$

Overall energy conversion efficiency of the trigeneration system is defined by:

$$\eta_{tri} = \frac{W_{sofc} + W_{GT} + W_T + Q_E + Q_H - W_{comp} - W_{pump}}{\dot{m}_{fuel} \cdot LHV} \quad (55)$$

Table 1
Conditions of simulation for the proposed CCHP system driven by SOFC.

Term	Value
Ambient temperature	293.15 K
Ambient pressure	1.013 bar
Fuel compressor isentropic efficiency	85%
Air compressor isentropic efficiency	85%
SOFC operating pressure	8.104 bar
Inlet temperature to the SOFC	700 K
Minimum steam-to-carbon ratio	2
Fuel utilization factor	0.85
DC-AC inverter efficiency	90%
Active surface area	220 cm^2
Number of cell	50,000
Exchange current density of anode	0.3 A cm^{-2}
Exchange current density of cathode	0.075 A cm^{-2}
Thickness of the anode	0.01 cm
Thickness of the cathode	0.19 cm
Thickness of the interconnect	0.0085 cm
Thickness of the electrolyte	0.004 cm
After-burner combustion efficiency	99%
Gas turbine efficiency	75%
Pump efficiency	80%
Ammonia–water turbine inlet pressure	100 bar
Ammonia concentration entering ammonia–water turbine	0.45
Ammonia–water turbine extraction ratio	0.5
Ammonia–water turbine efficiency	85%
Extraction ratio for heat provision	0.5
Extraction pressure from ammonia–water turbine	33.3 bar
Pinch point temperature difference	10 K

5. Results and discussion

A new CCHP system driven by SOFC is proposed by integrating an ammonia–water thermodynamic cycle with a SOFC-GT system to perform the trigeneration using methane as fuel. Prior to any practical experience with any new process, a comprehensive theoretical study must be done in order to assess the performance of the new technology or combination of existing technologies. Thus, the proposed CCHP system is simulated under steady-state conditions based on a mathematical model. Thermodynamic properties of the ammonia–water mixture were calculated by a convenient semi-empirical method, which combined the Gibbs free energy method for single phase [28] and empirical correlations for phase equilibrium [29]; the differences between calculated data and experimental data were less than 0.3% with good agreement [30].

The conditions of simulation for the new CCHP system driven by SOFC are summarized in Table 1. Tables 2 and 3 list the thermodynamic parameters at each node of the proposed CCHP system, and Table 4 shows the results of thermodynamic simulation. The overall energy conversion efficiency of the CCHP system reaches about 82% under the given conditions, and it also can be further improved by parameter optimization.

Table 3
Results of simulation for the bottoming cycle.

State	T (K)	p (bar)	X	$\dot{m}$ (kg s^{-1})	h (kJ kg^{-1})	s (kJ kg^{-1} K^{-1})
1	799.00	100	0.45	0.510	3098.19	6.6456
2	384.26	1.279	0.45	0.255	2192.64	7.0789
3	358.09	1.279	0.45	0.255	1687.89	5.6961
4	298.15	1.279	0.35	0.714	−97.67	0.2755
5	656.13	30	0.45	0.255	2765.51	6.7363
6	475.06	30	0.45	0.255	2004.61	5.2938
7	313.00	30	0.45	0.255	−55.55	0.4441
8	288.11	1.279	0.45	0.255	−55.55	0.4684
9	298.16	10	0.35	0.283	−96.50	0.2752
10	424.66	10	0.10	0.297	580.98	1.9122
11	374.26	10	0.35	0.283	358.98	1.5957
12	363.65	1.279	0.10	0.204	580.98	1.9776
13	449.82	10	0.10	0.093	2668.22	6.6151
14	303.41	10	0.99	0.141	1303.22	4.3751
15	298.25	10	0.99	0.063	117.50	0.4241
16	298.25	10	0.99	0.079	117.50	0.4241
17	260.51	2.411	0.99	0.079	117.50	0.4972
18	278.82	2.411	0.99	0.079	1296.04	4.9922
19	298.16	2.411	0.35	0.432	−97.58	0.2757
20	298.15	2.411	0.45	0.510	−123.75	0.2316
21	299.30	100	0.45	0.510	−109.35	0.2403

Table 4
The simulation results of the proposed CCHP system.

Term	Value
SOFC operating temperature	1220 K
After-burner combustion temperature	1407 K
Ammonia–water turbine inlet temperature	799 K
Cell operating voltage	0.665 V
SOFC operating current density	3691 A m^{-2}
SOFC electrical power	2432 kW
Air compressor power	544 kW
Fuel compressor power	419 kW
Pump1 power	0.195 kW
Pump2 power	0.414 kW
Pump3 power	0.049 kW
Pump4 power	1.415 kW
Gas turbine power	1468 kW
Ammonia–water turbine power	316 kW
Heat output	525 kW
Refrigeration output	93 kW
SOFC electricity efficiency	46.73%
Electricity efficiency of the system	69.73%
Overall energy conversion efficiency	81.61%

Table 2
Results of simulation for SOFC-GT system.

State	T (K)	p (bar)	$\dot{n}$ (mol s^{-1})	Molar flow rate (mol s^{-1})						
				CH_4	N_2	O_2	H_2	CO	CO_2	H_2O
a	293.15	1.013	77.78	0	61.44	16.33	0	0	0	0
b	293.15	1.013	6.50	6.5	0	0	0	0	0	0
c	293.15	1.013	13	0	0	0	0	0	0	13
d	569.69	8.106	77.78	0	61.44	16.33	0	0	0	0
e	485.99	8.106	6.50	6.5	0	0	0	0	0	0
f	293.17	8.106	13	0	0	0	0	0	0	13
g	700.00	8.106	77.78	0	61.44	16.33	0	0	0	0
h	700.00	8.106	19.50	6.5	0	0	0	0	0	13
i	1220.00	8.106	67.26	0	61.44	5.81	0	0	0	0
j	1220.00	8.106	32.50	0	0	0	3.71	1.24	5.26	22.29
k	1407.00	8.106	97.28	0	61.44	3.33	0	0	6.5	26
l	1062.00	1.013	97.28	0	61.44	3.33	0	0	6.5	26
m	988.00	1.013	97.28	0	61.44	3.33	0	0	6.5	26
n	966.00	1.013	97.28	0	61.44	3.33	0	0	6.5	26
o	819.00	1.013	97.28	0	61.44	3.33	0	0	6.5	26
p	353.24	1.013	97.28	0	61.44	3.33	0	0	6.5	26

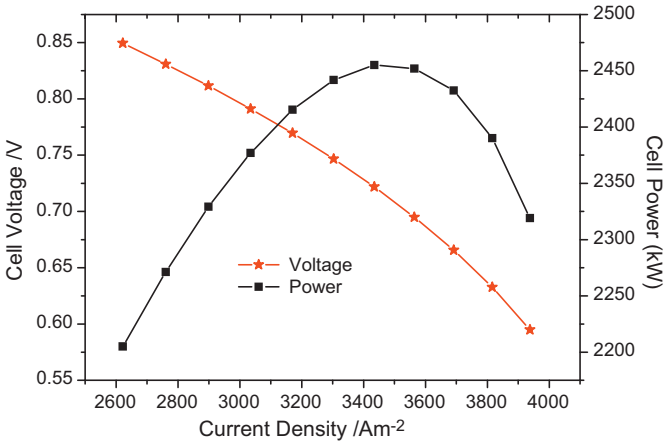

Fig. 3. Cell voltage vs. current density.

Some key parameters can influence the performance of the overall CCHP system, such as fuel flow rate, compressor pressure ratio, ammonia–water turbine inlet pressure, and basic solution ammonia–water concentration. Therefore, it is necessary to achieve the parameter analysis to evaluate the effects of each key parameter on the system performance of the CCHP system. In the parametric analysis, one parameter is varied, whereas others are kept constant as those in Table 1.

Fig. 3 shows the relationship between the cell voltage and its current density. As the current density increases, the cell voltage decreases due to typical losses in the fuel cell. But the cell power increases at first, and decreases later after reaching the peak value of 3500 A m^{-2}.

Fig. 4 shows the effect of fuel flow rate on the power of main components. In constant fuel utilization, increased fuel flow implies converting more chemical energy into electrical energy, which means more cells current being produced. As the cell current increases, and the cell voltage decreases, a maximum SOFC power, therefore, exists. Increased fuel flow leads to an increase in the temperature of combustion gas in the after-burner. Thus, the gas turbine power increases correspondingly. The compressor power consumption also rises due to increasing flow across the compressor. It is also found that the ammonia–water turbine power, heat output and refrigeration output all increase as the fuel flow rate increases. It is because that the temperature of exhaust from gas turbine can be elevated with the increasing fuel flow rate, resulting

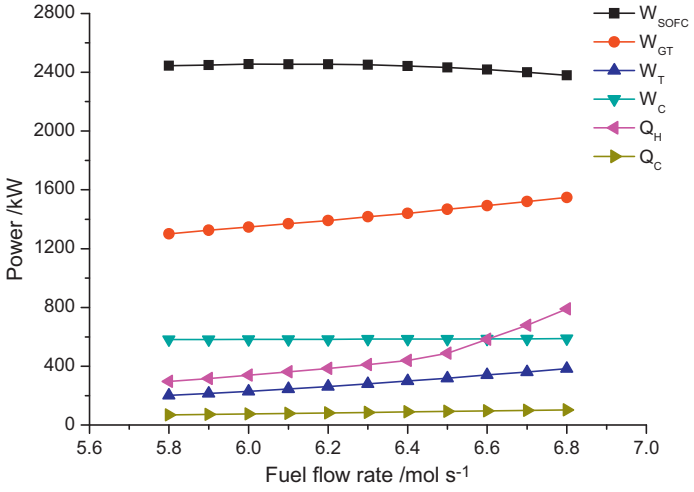

Fig. 4. Effect of fuel flow rate on the power of main components.

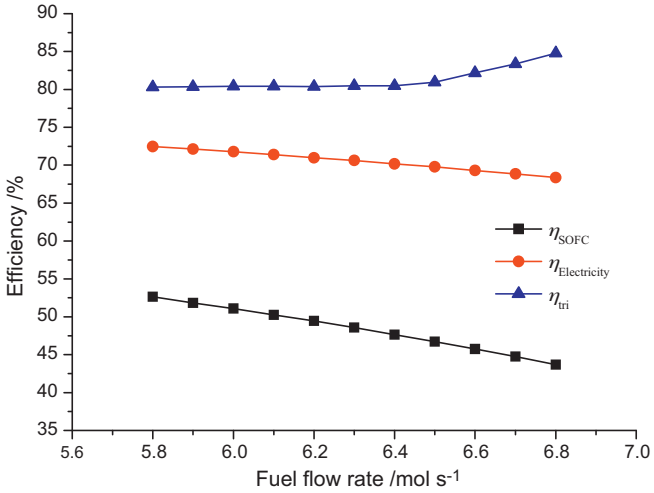

Fig. 5. Effect of fuel flow rate on the performance of system.

in an increase in the temperature of the exhaust entering waste heat boiler. Therefore, the bottoming cycle could utilize more waste heat to produce more power, cooling and heat through ammonia–water turbine, evaporator and heater.

Fig. 5 reveals the effect of fuel flow rate on the performance of system. It can be seen that as the fuel flow rate increases, both the SOFC efficiency and electricity efficiency decrease. Increased fuel flow rate has a negative effect on the SOFC efficiency and electricity efficiency. On the contrary, overall energy conversion efficiency of the trigeneration system increases with the increasing fuel flow rate because of a sharp increase in heat output from the CCHP system.

Fig. 6 shows the effect of compressor pressure ratio for air and CH_4 on the power of the main components. As the compressor pressure ratio increases, the cell voltage elevates correspondingly, resulting in an increase in power output of the SOFC. It is obvious that both gas turbine power output and compressor power input increase correspondingly owing to the increasing pressure ratio across the gas turbine and compressor. It is also found that the ammonia–water turbine power, heat output and refrigeration output all decrease as the compressor pressure ratio increases. It is because that the temperature of exhaust from gas turbine reduces with the increasing compressor pressure ratio, resulting in a decrease in the temperature of the exhaust gas entering the waste heat boiler. Thus, the bottoming cycle only utilizes less waste heat

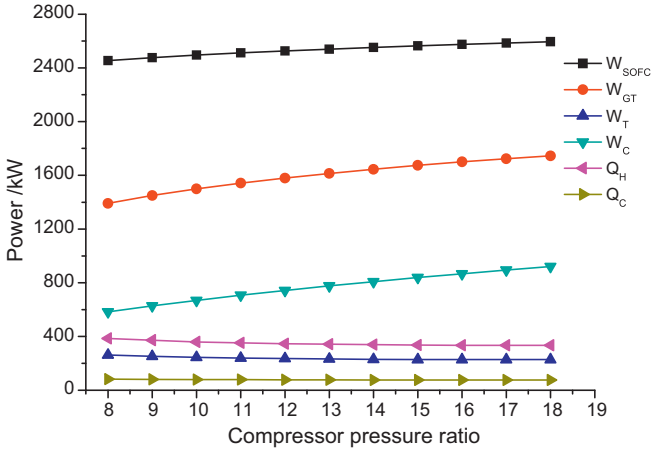

Fig. 6. Effect of compressor pressure ratio on the power of main components.

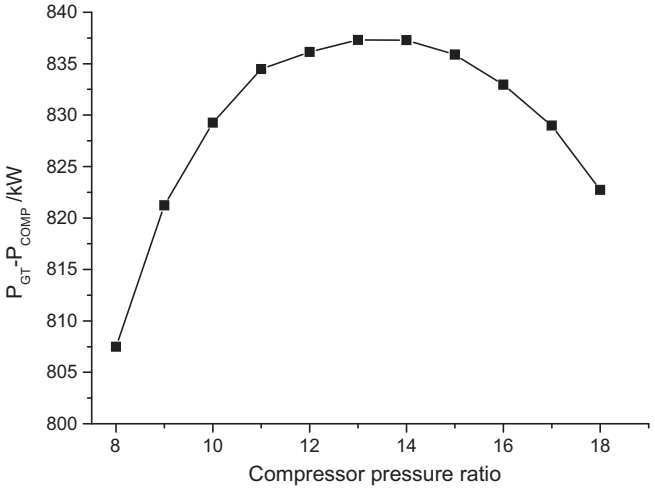

Fig. 7. Effect of compressor pressure ratio on the power difference between gas turbine and compressors.

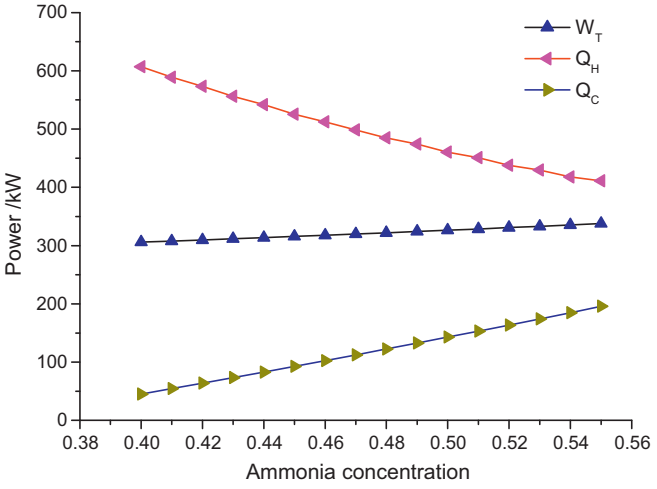

Fig. 9. Effect of ammonia concentration entering ammonia–water turbine on the power of some main components.

to produce less power, cooling and heat through ammonia–water turbine, evaporator and heater.

Fig. 7 shows the effect of compressor pressure ratio on the power difference between the gas turbine and compressors. It can be seen that there exists an optimal compressor pressure ratio to lead to a maximum power difference between the gas turbine and compressors.

Fig. 8 indicates the effect of compressor pressure ratio on the performance of system. It can be seen that as the compressor pressure ratio increases, the SOFC efficiency, electricity efficiency and overall energy conversion efficiency of the trigeneration system all increase in the given range of compressor pressure ratio. Although there exists an optimal compressor pressure ratio maximizing the power difference between the gas turbine and compressors and the ammonia–water turbine power decreases, a sharp increase in the SOFC power results in a smooth increase in the electricity efficiency with the increasing compressor pressure ratio.

It is obvious that the ammonia concentration entering ammonia–water turbine has no effects on the SOFC power, gas turbine power and compressor power under the given conditions. The effect of ammonia concentration entering ammonia–water turbine on the power of some main components is shown in Fig. 9. It can be seen that as the ammonia concentration entering ammonia–water turbine increases, both ammonia–water turbine power and refrigeration output increase, but heat output, on the contrary, decreases. It is shown in Fig. 10 that as the ammonia concentration increases, the electricity efficiency increases due to the increasing ammonia–water turbine power, and the overall energy conversion efficiency of the trigeneration system decreases first and then increases due to the combined effects of electricity output, heat output and refrigeration output of the proposed system.

It is also obvious that ammonia–water turbine inlet pressure has no effects on the SOFC power, gas turbine power and compressor power under the given conditions. Fig. 11 depicts the effect of ammonia–water turbine inlet pressure on the power of some main components. As ammonia–water turbine inlet pressure increases, mass flow rate of ammonia–water vapor produced in waste heat boiler decreases, resulting in a decrease in mass flow rate cross ammonia–water turbine. It is known that the enthalpy drop across the turbine increases as ammonia–water turbine inlet pressure increases. The enthalpy gain could make up for a decrease in mass flow rate through the turbine, and this leads to an increase in ammonia–water turbine power. The heat output decreases due to a decrease in extraction flow rate. In addition, ammonia–water turbine inlet pressure has little effect on the refrigeration output of the proposed system.

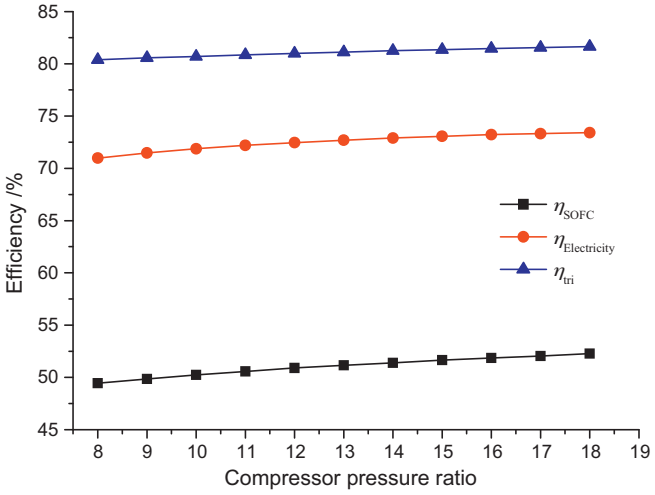

Fig. 8. Effect of compressor pressure ratio on the performance of system.

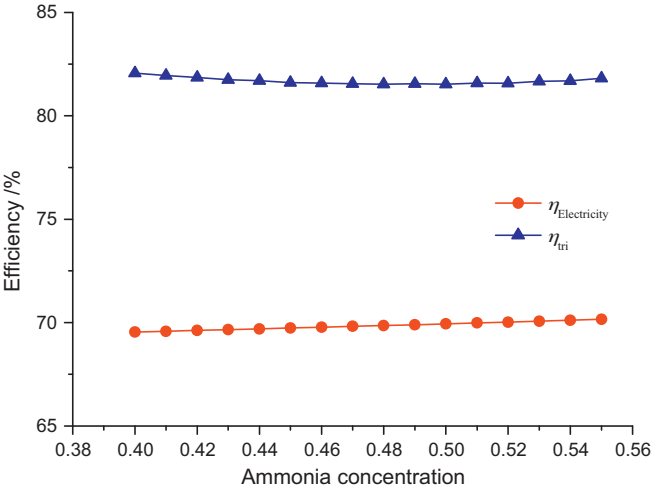

Fig. 10. Effect of ammonia concentration entering ammonia–water turbine on the performance of system.

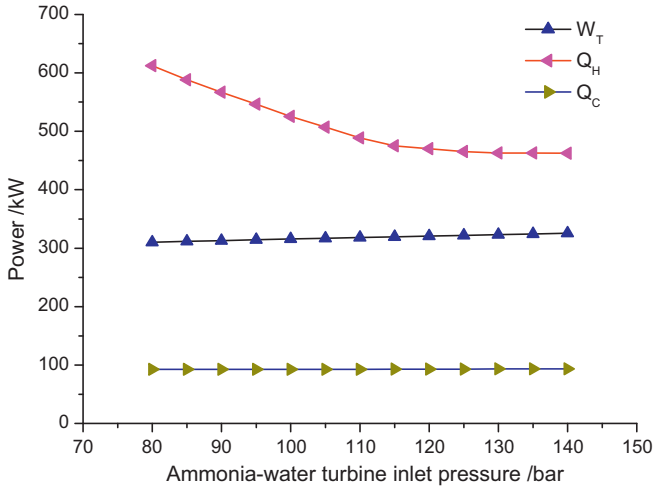

Fig. 11. Effect of ammonia–water turbine inlet pressure on the power of some main components.

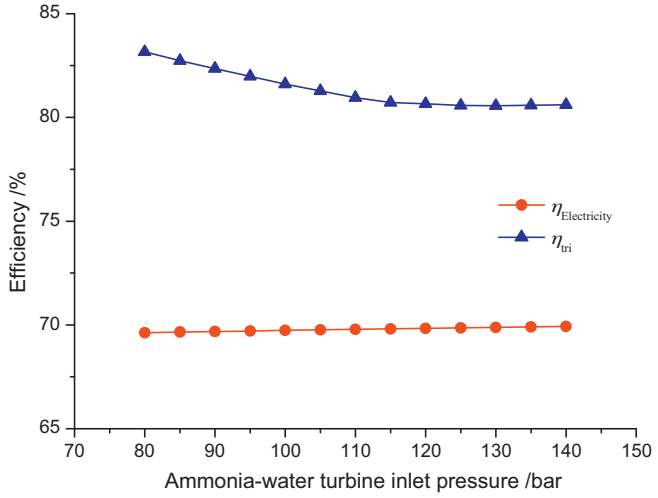

Fig. 12. Effect of ammonia–water turbine inlet pressure on the performance of system.

Fig. 12 shows the effect of ammonia–water turbine inlet pressure on the performance of system. As the ammonia–water turbine inlet pressure increases, the electricity efficiency increases due to the increasing ammonia–water turbine power, and overall energy conversion efficiency of the trigeneration system decreases due to a sharp decrease in heat output from the CCHP system.

The proposed CCHP system driven by SOFC is a new concept to perform the trigeneration. It uses methane as fuel, and can be easily extended to use other fuel, such as hydrogen. The thermo-economical analysis is required to evaluate the cost of system. The experimental study is also necessary to validate the feasibility of the proposed CCHP system in the future.

6. Conclusions

In order to elevate the conventional energy conversion efficiency, the main objective of the present study is to propose a new CCHP system driven by solid oxide fuel cell using ammonia–water mixture to recover the waste heat from the SOFC-GT to solve the energy and environment problems and to meet diverse energy requirements for users. This proposed system combines a SOFC-GT system and a new bottoming cycle using ammonia–water mixture to produce cooling output, heating output and power output simultaneously. The main conclusions drawn from present study are summarized as follows:

(1) The overall energy conversion efficiency of the proposed CCHP system driven by SOFC can exceed 80% under the given conditions.
(2) Increasing the fuel flow rate results in a decreasing SOFC efficiency and electricity efficiency, whereas it improves overall energy conversion efficiency of the trigeneration system.
(3) SOFC efficiency, electricity efficiency and overall energy conversion efficiency of trigeneration system can be improved by increasing the compressor pressure ratio.
(4) High ammonia concentration entering ammonia–water turbine has a positive effect on the electricity efficiency, and there is an optimal value of ammonia concentration in terms of minimizing the overall energy conversion efficiency of the trigeneration system due to the combined effects of trigeneration output.
(5) High ammonia–water turbine inlet pressure has a positive effect on the electricity efficiency; on the other hand, it has a negligible effect on the overall energy conversion efficiency.

Acknowledgement

The authors gratefully acknowledge the financial support of The National High Technology Research and Development Program (863 Program) of China (Grant No. 2009AA05Z205).

References

[1] D. Wu, R. Wang, Prog. Energy Combust. 32 (2006) 459–495.
[2] J. Palsson, A. Selimovic, L. Sjunnesson, J. Power Sources 86 (2000) 442–448.
[3] P. Cosramagna, L. Magistri, A.F. Massardo, J. Power Sources 96 (2001) 352–368.
[4] A.F. Massardo, F. Lubelli, ASME J. Eng. Gas Turb. Power 122 (2000) 27–35.
[5] S.H. Chan, H.K. Ho, Y. Tian, J. Power Sources 111 (2002) 320–328.
[6] S.H. Chan, H.K. Ho, Y. Tian, J. Power Sources 114 (2003) 213–227.
[7] F. Calise, A. Palombo, L. Vanoli, J. Power Sources 158 (1) (2006) 225–244.
[8] F. Calise, M.D. d'Accadia, L. Vanoli, M.R. von Spakovsky, J. Power Sources 159 (2006) 1169–1185.
[9] W.J. Yang, S.K. Park, T.S. Kima, J.H. Kim, J.L. Sohn, S.T. Ro, J. Power Sources 60 (2006) 462–473.
[10] S.K. Park, K.S. Oh, T.S. Kim, J. Power Sources 170 (2007) 130–139.
[11] W.H. Lai, C.A. Hsiao, C.H. Lee, Y.P. Chyou, Y.C. Tsai, J. Power Sources 171 (2007) 130–139.
[12] P.G. Bavarsad, Int. J. Hydrogen Energy 32 (2007) 4591–4599.
[13] A.V. Akkaya, B. Sahin, H.H. Erdem, Int. J. Hydrogen Energy 33 (2008) 2566–2577.
[14] Y. Haseli, I. Dincer, G.F. Naterer, Int. J. Hydrogen Energy 33 (2008) 5811–5822.
[15] W. Burbank Jr., D. Witmera, F. Holcomb, J. Power Sources 193 (2009) 656–664.
[16] C. Bao, Y.X. Shi, E. Croiset, C. Li, N.S. Cai, J. Power Sources 195 (2010) 4871–4892.
[17] V. Verda, J. Fuel Cell Sci. Technol. 5 (2008).
[18] A.V. Akkaya, B. Sahin, Int. J. Energy Res. 33 (2009) 553–564.
[19] M. Burer, K. Tanaka, D. Favrat, K. Yamada, Energy 28 (2003) 497–518.
[20] Y Liu, K.C. Leong, J. Power Sources 159 (2006) 501–508.
[21] Z.T. Yu, J.T. Han, X.Q. Cao, W. Chen, B. Zhang, Int. J. Hydrogen Energy 35 (2010) 2703–2707.
[22] F.A. Al-Sulaiman, I. Dincer, F. Hamdullahpur, Int. J. Hydrogen Energy 35 (2010) 5104–5113.
[23] F.A. Al-Sulaiman, I. Dincer, F. Hamdullahpur, J. Power Sources 195 (2010) 2346–2354.
[24] A.I. Kalina, ASME J. Eng. Gas Turb. Power 106 (1984) 737–742.
[25] A.V. Akkaya, Int. J. Energy Res. 31 (2007) 79–98.
[26] R.P. O'Hayre, S.W. Cha, W. Colella, F.B. Prinz, Fuel cell Fundamentals, 2nd ed., John Wiley & Sons, Ltd., 2006.
[27] D.F. Che, Boilers-theory, Design and Operation, Xi'an Jiaotong University Press, 2008.
[28] B Ziegler, C. Trepp, Int. J. Refrig. 7 (1984) 101–106.
[29] Y.M. El-Sayed, M. Tribus, ASME Adv. Energy Syst. Div. 1 (1985) 89–95.
[30] F. Xu, D.Y. Goswami, Energy 24 (1999) 525–536.